Research Article | Vol. 26, No. 24 | 26 Nov 2018 | OPTICS EXPRESS 31925
Optics EXPRESS

Measuring azimuthal and radial modes of photons

FRÉDÉRIC BOUCHARD,[1,*] NATALIA HERRERA VALENCIA,[2,3] FLORIAN BRANDT,[2,4] ROBERT FICKLER,[2] MARCUS HUBER,[2] AND MEHUL MALIK[2,4]

[1] *Department of Physics, University of Ottawa, 25 Templeton Street, K1N 6N5, Ottawa, Canada*
[2] *Institute for Quantum Optics and Quantum Information (IQOQI), Austrian Academy of Sciences, Boltzmanngasse 3, A-1090 Vienna, Austria*
[3] *Université dÁix-Marseille, Centre de Saint-Jérôme, 13014, Marseille, France*
[4] *Institute of Photonics and Quantum Sciences (IPaQS), Heriot-Watt University, EH14 4AS, Edinburgh, UK*
[*] *fbouc052@uottawa.ca*

Abstract: With the emergence of the field of quantum communications, the appropriate choice of photonic degrees of freedom used for encoding information is of paramount importance. Highly precise techniques for measuring the polarisation, frequency, and arrival time of a photon have been developed. However, the transverse spatial degree of freedom still lacks a measurement scheme that allows the reconstruction of its full transverse structure with a simple implementation and a high level of accuracy. Here we show a method to measure the azimuthal and radial modes of Laguerre-Gaussian beams with a greater than 99 % accuracy, using a single phase screen. We compare our technique with previous commonly used methods and demonstrate the significant improvements it presents for quantum key distribution and state tomography of high-dimensional quantum states of light. Moreover, our technique can be readily extended to any arbitrary family of spatial modes, such as mutually unbiased bases, Hermite-Gauss, and Ince-Gauss. Our scheme will significantly enhance existing quantum and classical communication protocols that use the spatial structure of light, as well as enable fundamental experiments on spatial-mode entanglement to reach their full potential.

1. Introduction

Photons have long been a candidate of choice for many proof-of-principle experiments in quantum communications, quantum information processing, and foundations of quantum mechanics [1]. For several decades, due to its maturity in generation and detection, the polarization of photons has now become a standard experimental resource for fundamental and applied experiments, and, to this day, is still being used in a wide array of important experimental demonstrations [2–4]. Nevertheless, other photonic degrees of freedom, such as frequency and time [5, 6] or position and momentum [7], offer new, yet unexploited advantages where polarization encoding is limited. One advantage of these degrees of freedom is their high-dimensional nature, whereas polarization is inherently bidimensional, i.e. *qubits*. High-dimensional quantum systems, also known as *qudits*, are both interesting at the fundamental level and useful in applications such as quantum communications and cryptography [8, 9], offering an increased information capacity and greater resistance to noise [10].

A specific family of spatial modes that has gained a lot of attention in the last years is the azimuthal modes of Laguerre-Gauss (LG) beams. In particular, it was found that such solutions of the paraxial wave equation are related to an orbital angular momentum (OAM) proportional to the azimuthal mode index ℓ [11] and are characterized by a twisted helical wavefront of the form $\exp(i\ell\varphi)$, where φ is the azimuthal coordinate. Mathematically, these solutions have the

#342120 https://doi.org/10.1364/OE.26.031925
Journal © 2018 Received 14 Aug 2018; revised 7 Oct 2018; accepted 8 Oct 2018; published 19 Nov 2018

Optics EXPRESS

advantage of representing a set of complete and orthogonal functions, thus forming a convenient basis to expand any arbitrary azimuthal functions. Experimentally, OAM modes have been a fruitful testbed for experimental demonstrations in quantum entanglement [12, 13], quantum simulation [14] and QKD [15–17]. Due to their simple form, OAM states are readily generated using devices that shape the wavefront of an incoming beam. Spiral phase plates [18], pitch-fork gratings [19], spatial light modulators (SLM) [20], and q-plates [21] are examples of established devices to generate light beams carrying OAM. Nevertheless, none of the aforementioned techniques directly generate pure LG modes, due to difficulties in manipulating their radial component. Therefore, several generation techniques have been proposed and implemented for experimentally achieving pure LG modes. Among these, holographic amplitude-masking techniques modulating the amplitude and phase of a beam using a single phase-only SLM, although lossy, have been a useful experimental tool to generate any arbitrary desired modes with high precision [22, 23]. For instance, the amplitude modulated holograms may be straightforwardly displayed on an SLM, thus making the generation of LG modes simple and compact for table-top experiments.

Although the generation of spatial modes is relatively simple to realize, it is surprisingly not the case for their detection. A technique known as *phase-flattening* has been demonstrated and become the standard for measuring OAM states of light [24]. In this scheme, the incoming OAM beam that is to be measured is impinged onto a phase element and subsequently coupled to a single-mode fibre (SMF). For the detection of a given OAM value, a phase pattern with the opposite OAM is imprinted on the SLM, thereby flattening the phase of the incoming beam and allowing it to couple efficiently to the SMF. In all other cases, the resulting beam after the phase modulation will not match the fundamental mode of the SMF. In this way, the phase-flattening method can be used as a filter to measure the OAM content of an unknown incoming beam. This technique also possesses limitations where mode-dependent losses renders the detection of higher-order OAM states less efficient [25]. Nevertheless, phase-flattening has now become a standard method for measuring OAM and is also widely used in experiments utilizing OAM both in the classical and the quantum regime. In another approach, it is possible in principle to measure any arbitrary spatial modes with high accuracy using a large enough sequence of phase elements and free-space propagation separating the elements. For example, with this configuration, a mode sorter was realized using two phase elements [26, 27], namely an unwrapper and a phase corrector. A sorter-type scheme has the advantage of being able to measure the OAM value of the incoming beam in a single shot, rendering the detection scheme more efficient. Moreover, when considering a larger number of phase elements, a larger flexibility allows one to perform a measurement over a much larger number of modes [28] or to carry out mode transformations [29]. However, as the number of phase elements increases, small imperfections in alignment leads to significant mode cross-talks and limits the practicality of such implementations.

Here, we propose and experimentally demonstrate a method that we refer to as *intensity-flattening*. Our method extends the well-established phase-flattening method and enables us to measure arbitrary spatial modes using a simple experimental configuration that requires a single hologram. With a reasonable amount of loss, our method enables us to measure spatial modes with extremely small crosstalk values corresponding to a visibility larger than 99 %. This technique will be useful for fundamental, proof-of-concept experiments and all tasks where high-quality measurements are necessary and losses can be tolerated.

2. Theory

Let us set the stage by writing out the orthogonality condition for the Laguerre-Gauss functions, i.e.

Optics EXPRESS

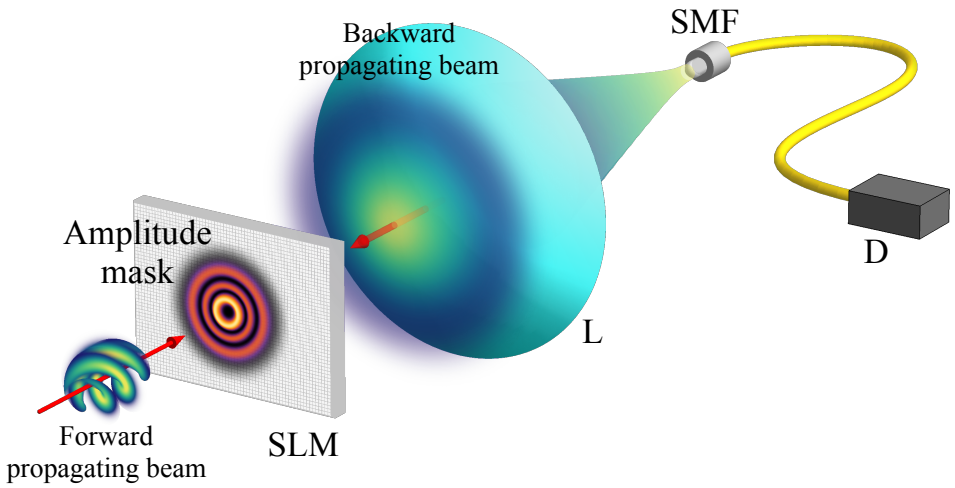

Fig. 1. Simplified experimental setup. A forward-propagating beam with an unknown spatial mode is made incident on a spatial light modulator (SLM). A hologram simultaneously modulating the phase and the amplitude of the incoming beam is displayed on the SLM. Subsequently, the outgoing beam is coupled to a single-mode fibre (SMF) after passing through a set of lenses and microscope objectives (not shown). The choice of lenses can be understood by considering a back-propagating beam exiting the SMF and made incident on the SLM from the back. According to the intensity-flattening technique presented here, this beam should be expanded on the SLM in order to flatten the intensity distribution of the Gaussian component.

$$\int_0^{2\pi}\int_0^{\infty} \mathrm{LG}^*_{\ell',p'}(r,\varphi)\,\mathrm{LG}_{\ell,p}(r,\varphi)\,r\mathrm{d}r\mathrm{d}\varphi \;=\delta_{\ell\ell'}\,\delta_{pp'}. \tag{1}$$

In the laboratory, an input LG beam, $\mathrm{LG}_{\ell,p}(r,\varphi)$, is generated using the previously mentioned amplitude-masking method on a first SLM. The beam is now made incident on a second SLM which is displaying the mode $\mathrm{LG}^*_{\ell',p'}(r,\varphi)$, also using the amplitude-masking technique. Finally, the beam is made to couple to an SMF and the coupled intensity or photon counts are recorded. Due to the unitarity of free-space propagation, we have the freedom to choose at which point we calculate the overlap integral after the SLMs. Thus we imagine a backward propagating beam from the SMF to the second SLM. This experimental scenario corresponds to the overlap integral,

$$\int_0^{2\pi}\int_0^{r_{\max}} \mathrm{LG}^*_{\ell',p'}(r,\varphi)\,\mathrm{LG}_{\ell,p}(r,\varphi)\,e^{-r^2/w_0^2}\,r\mathrm{d}r\mathrm{d}\varphi \;\neq\delta_{\ell\ell'}\,\delta_{pp'}, \tag{2}$$

where $r_{\max}$ takes into account finite numerical apertures in the experiment and w_0 is the beam waist of the SMF. We note that this integral is different from the overlap integral of LG modes, Eq. (1), due to the additional gaussian factor of the SMF [30, 31]. The aim of our method is to remove the effect of this Gaussian factor to retrieve the standard orthogonality relation of LG beams. A simple but very effective way of achieving this, is by increasing the value of the backward propagating beam waist, w_0, in Eq. (2). For a large enough w_0, from the perspective of the LG terms in the integral, the additional Gaussian factor will appear flat over the region of interest, thus retrieving Eq. (1). This intensity-flattening technique requires minimal

Optics EXPRESS

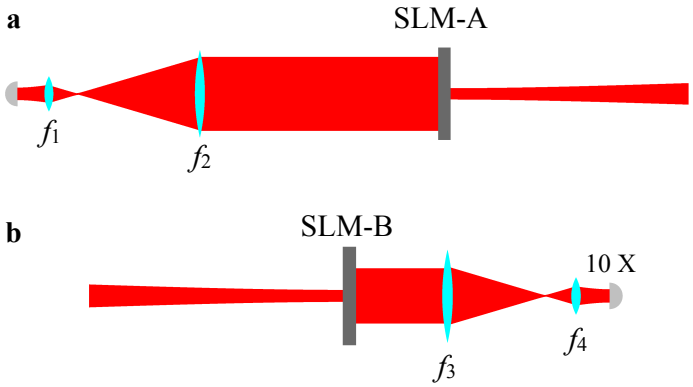

Fig. 2. Experimental details. (a) An attenuated laser diode is enlarged using a telescope with a magnification of f_2/f_1 = (300 mm)/(50 mm) = 6. The beam is then made incident on a first spatial light modulator (SLM-A) which reflects the incoming beam (shown in transmission here for simplicity). The output beam has the desired intensity and phase profile after passing through a $4-f$ system that filters out the first order of diffraction (not shown here). (b) The beam that is to be measured is made incident on SLM-B. By considering a virtually backward-propagating beam from the 10X object, the set of lenses f_3 = 200 mm and f_4 = 50 mm magnifies the backward-propagating by a factor of 4, making its beam waist much larger than the beam waist of the detection mode on the SLM-B.

modifications to standard experimental setups measuring optical spatial modes, and allows one to select the appropriate trade-off between mode visibility and losses by tuning the beam waist, see Fig. 1. In order to demonstrate this powerful idea experimentally, we build a simple experimental setup allowing us to test our intensity-flattening method in several scenarios – measuring radial modes, key rates in QKD, and quantum state tomography. We also investigate and compare the performance of the intensity-flattening technique when considering beams other than Gaussian, such as flat-top and exponential, which can be seen in the appendix-a.

3. Experimental setup

An attenuated diode laser at a wavelength of 810 nm is coupled to an SMF to clean its spatial profile to the fundamental Gaussian mode. The beam is coupled out of the SMF using a collimator resulting in a beam with a $1/e^2$ beam waist of 1.1 mm, which is then enlarged using a telescope with a magnification of f_2/f_1 = (300 mm)/(50 mm) = 6, where f_1 and f_2 are the focal length of the first and the second lens in the telescope, respectively. The large collimated beam is made incident on SLM-A where the desired spatial mode is generated using an amplitude-masking technique [23]. The beam waist of the mode displayed on SLM-A is given by w_0 = 500 μm. A $4f$-system is then used in order to filter out the first order of diffraction and to image SLM-A onto SLM-B. The beam is then sent through a second telescope with a magnification of f_4/f_3 = (50 mm)/(200 mm) = 0.25 and then coupled to an SMF using a 10-X microscope objective. The choice of f_3 and f_4 becomes clearer when considering the backward-propagating beam, (Fig. 1), where the effect of the telescope is to enlarge the size of the backward-propagating beam on SLM-B to 4.2 mm, hence increasing the beam waist of the Gaussian factor in Eq. (2). A more detailed experimental setup is shown in Fig. 2.

Optics EXPRESS

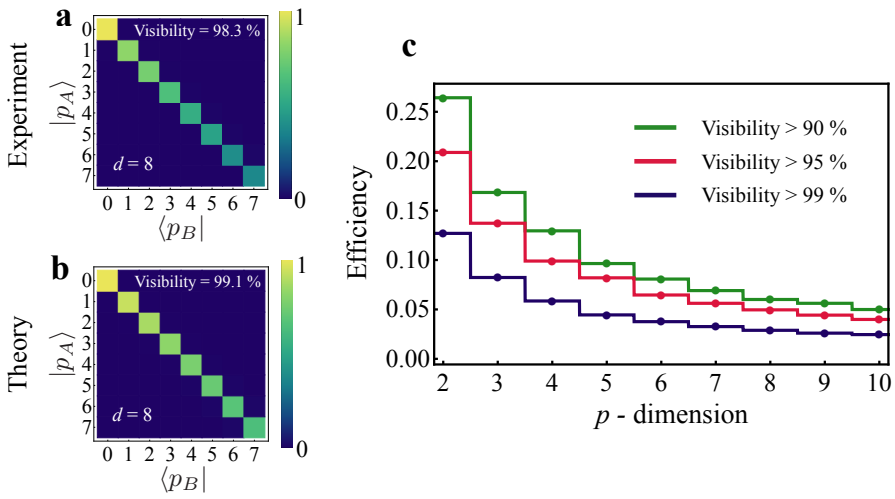

Fig. 3. Measurement of radial modes. (a) Experimentally measured and (b) simulated cross-talk matrix of radial modes ranging from $p = 0$ to $p = 7$ in a prepare-and-measure setting. The cross-talk matrix is normalized to unity by dividing each elements by the element with maximum counts. The rows and the columns correspond to the states, $|p_A\rangle$ and $|p_B\rangle$, prepared and measured by Alice and Bob, respectively. A visibility of $V = 98.3$ % is obtained from the experimentally measured cross-talk matrix. In theory, a visibility in excess of 99 % is achieved by considering a back-propagating with a beam waist 5.4 times larger than that of the beam waist of the detection mode of the holograms. (c) The efficiency of the intensity-flattening measurement technique is shown as a function of dimensionality of radial modes. For a dimension of d, radial modes ranging from $p = 0$ to $p = d - 1$ are considered. For each dimensions, the reported efficiencies are obtained by increasing the beam waist of the back-propagating up to the point where visibilities are in excess of 99 % (dark blue), 95 % (red) and 90 % (green).

4. Radial modes

As a first experimental demonstration of our technique, let us consider the radial modes of the LG beams. These modes have recently been investigated both theoretically and experimentally in the context of quantum information [31–35] and play a key role in fully utlizing the information-carrying capacity of a photon. Since then, several experimental techniques have been proposed to measure radial modes in a sorter configuration, i.e. using a scattering medium [36] or taking advantage of the p-dependent Gouy phase in an interferometric configuration [37, 38]. Such schemes have the advantage of having a higher detection efficiency in principle compared to a filter-type measurement as we propose. Nevertheless, in the first case, low transmission efficiencies prohibit its use in a realistic quantum experiment and in the second case, the stability and interferometric nature of the implementation makes these techniques challenging. In contrast, our method has the advantage of being simple, compact and stable for measuring radial modes. In order to demonstrate the quality of measurements achievable with our method, we measure the cross-talk among radial modes ranging from $p = 0$ to 7 using our intensity-flattening technique, see Fig. 3. The modal cross-talk is characterized by considering the visibility of the cross-talk matrix, which we define as $V = \sum_i C_{ii} / \sum_{ij} C_{ij}$, where C_{ij} corresponds to the cross-talk matrix. For an 8-dimensional radial mode subspace, we experimentally obtain a visibility value of $V = 98.3$ %, which is the highest experimentally achieved value so far reported (to the best of our knowledge).

Optics EXPRESS

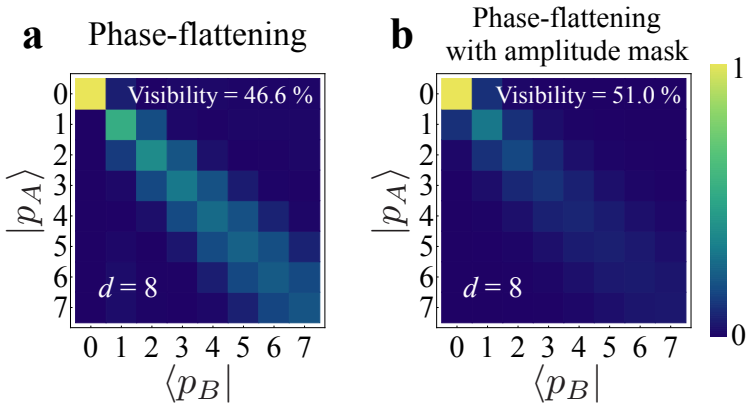

Fig. 4. Performance of phase-flattening in measuring radial modes. Simulated cross-talk matrix of radial modes measurement with (a) a phase-flattening measurement scheme and (b) a phase-flattening with amplitude mask measurement scheme.

We note that we may observe a mode-dependent efficiency in our measurements, which is attributed to the overall transmission of the amplitude mask due to the geometry of the imprinted modes, as well as the coupling to the SMF. This effect is also seen from the theory, see Fig. 3-(**b**), and can be straightforwardly compensated for. In order to achieve a visibility of 98.3 %, the beam waist of the virtually backward propagating beam has been chosen to be 8.4 times larger than the beam waist of the generation and measurement holograms. We experimentally measured the average efficiency of detection to be 3.2 %, for radial modes ranging from $p = 0$ to 7, where losses due to the amplitude mask and coupling to the single mode fibre are taken into account. In theory, for an 8-dimensional radial mode subspace, a visibility in excess of 99 % is achieved by enlarging the backward-propagating beam by a factor of 5.4.

By varying the size of the back-propagating beam on SLM-B we may achieve, in theory, arbitrarily high visibility values at the cost of an increase in loss. However, we demonstrate that high visibility may still be achieved with reasonable losses, rendering this technique useful for a broad range of experiments. In general, when considering higher-order modes and thus larger dimensional states, enlarged beam waists w_0 must be considered for a similar visibility value. In order to show this effect, we calculate the detection efficiency resulting from increasing the beam waist of the back-propagating beam for obtaining visibility values that are larger than 90 %, 95 % and 99 %, for several dimensions of radial subspaces, see Fig. 3-(**c**). We note that in the case of a 10-dimensional subspace, i.e. $p = 0$ to 9, a visibility larger than 99 % is achieved with an efficiency of 2.5 %, which is often tolerable in quantum information processing as well as classical application tasks. For the case of spontaneous parametric downconversion, coincidence count rates, summed over all modes, on the order of 10^5 Hz may be expected for a typical implementation [12]. If one were to use the intensity-flattening technique to measure pairs of entangled photons, coincidence count rates on the order of 10^2 to 10^3 Hz can be expected. We further note that our technique has the advantage of allowing the user to vary w_0 at will in order to obtain a certain visibility for a tolerable efficiency.

In order to compare our intensity-flattening with a previously established measurement technique, we investigate the performance of phase-flattening in measuring radial modes. In particular, we consider two strategies where the beam waist of the backward-propagating beam is fixed to w_0, where w_0 is the beam waist of the generated and detected modes on the holograms of the spatial light modulators (SLM). In the first case, a phase-only hologram is employed at the

Optics EXPRESS

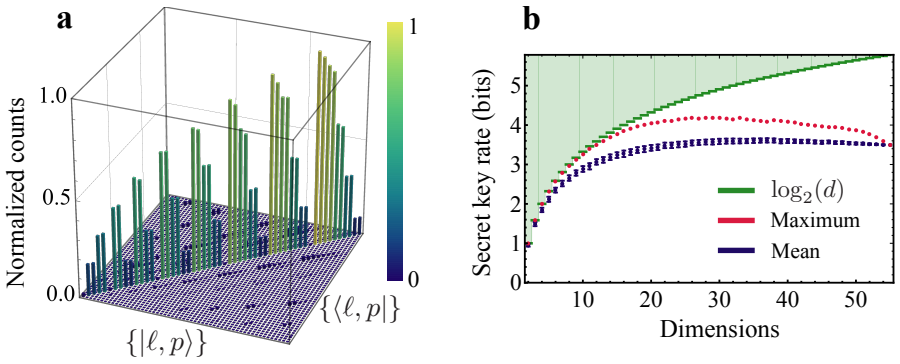

Fig. 5. Measurement of a 55-dimensional space using azimuthal and radial modes. (a) Experimentally measured cross-talk matrix for a 55-dimensional space of azimuthal and radial modes. In order to show mode-dependent efficiencies, the cross-talk matrix is normalized to unity by dividing each elements by the element with maximum counts. The list of states $\{|\ell, p\rangle\}$ are given explicitly in the appendix-c. (b) Secret key rates obtained from lower dimensional subspaces of the full 55-dimensional space. For a given subspace, a sample of 1000 different combinations is selected. For each combination of subspaces, a secret key rate is calculated from the experimental data. The mean and the standard deviation of the secret key rates over the 1000 combinations are shown in dark blue. The maximal secret key rates obtained by searching for the optimal subspace using a genetic algorithm are shown in red. The theoretical maximal values are shown in green, given by $\log_2(d)$. The shaded region corresponds to values of secret key rates inaccessible for the corresponding dimensions.

detection SLM. The corresponding phase of the mode to detect is displayed flattening the phase of the outgoing beam. However, the overlap of the phase-flattened beam with the single mode fibre leads to a modal cross-talk in the measurement of radial modes. In dimension 8, a visibility of $V = 46.6$ % is obtained from the calculated cross-talk matrix of radial modes, see Fig. 4-(**a**).

Another possible strategy that we consider involves an amplitude mask, where the backward propagating beam's waist is also fixed to w_0. This technique also leads to a large modal cross-talk and mode-dependent losses. Nevertheless, in dimension 8, a visibility of $V = 51.0$ % is obtained from a calculated cross-talk matrix of radial modes, achieving a slightly higher visibility than the phase-only flattening technique, see Fig. 4-(**b**).

5. Full-field modes

As a second demonstration of our intensity-flattening method for measuring spatial modes, we consider the full-field structure of spatial modes, i.e. the joint azimuthal and radial degrees of freedom. The transverse spatial degree of freedom inherently requires two spatial coordinates to characterize the transverse plane, e.g. x and y in cartesian coordinates, or r and φ in polar coordinates. Thus in order to take full advantage of transverse spatial modes, it is becoming increasingly important to take into consideration both the azimuthal and radial modes when dealing with LG beams [39, 40]. However, due to the lack of a proper technique to measure arbitrary spatial modes in a feasible experimental implementation, only a few experiments have investigated azimuthal and radial modes jointly for quantum entanglement [12, 41] and for classical communications [42]. We now demonstrate how our intensity flattening can be applied in a full-field experiment by measuring states of light in both azimuthal and radial modes.

It has been shown repeatedly that high-dimensional states of light have various applications in

Optics EXPRESS

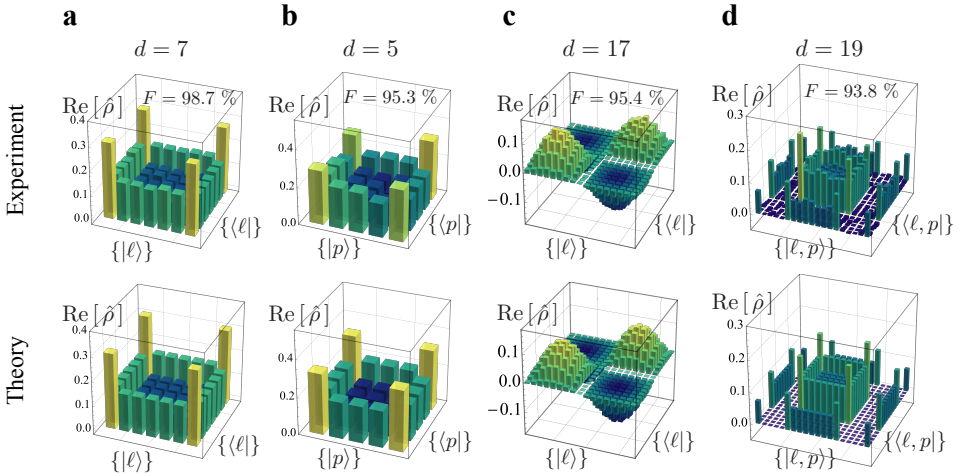

Fig. 6. High-dimensional quantum state tomography. The experimentally reconstructed density matrices for a (a) 7-dimensional OAM state, (b) 5-dimensional radial state, (c) 17-dimensional OAM state and (d) 19-dimensional full-field state, are shown in the upper row along with their corresponding theory density matrices, respectively. High-dimensional states giving rise to visually interesting density matrices were chosen in order to resemble (a)-(b) a castle, (c) a sine function, and (d) a palace, where the explicit forms of the generated states are given in appendix-d. Fidelities of $F = 98.7\ \%$, $95.3\ \%$, $95.4\ \%$, and $93.8\ \%$, and efficiencies of $4.7\ \%$, $5.5\ \%$, $8.3\ \%$, and $6.6\ \%$ were obtained experimentally for (a)-(d), respectively.

quantum information. However, in any experimental implementations, one is rapidly confronted with the trade-off between higher dimensions and obtaining high quality measurements [12, 43]. Therefore, for a given quantum information protocol, the optimal dimensionality in experiments dealing with spatial mode is rarely the highest achievable dimension. This is commonly due to the fact that higher-order spatial modes typically result in lower measurement quality due to the complexity of the modes, pixel resolutions, or truncation due to a finite numerical aperture. By taking advantage of the mode order given by $N = 2p + |\ell| + 1$, we consider a 55-dimensional space consisting of the 55 lowest order azimuthal and radial LG modes with mode order ranging from $N = 1$ to 10, see appendix-c for the list of states employed. A visibility of 92.3 % is experimentally obtained from the full 55-dimensional cross-talk matrix presented in Fig. 5-(**a**).

As mentioned previously, there is a trade-off in experiments between dimensionality and visibility. We now explore this interplay by considering lower dimensional subsets of the 55-dimensional cross-talk matrix shown in Fig. 5-(**a**). An example of a physical parameter that illustrates the trade-off between the dimensionality and the visibility is the secret key rate in a high-dimensional QKD setting. For example, the secret key rate of the high-dimensional BB84 protocol [8] is given by $R = \log_2(d) - 2h^{(d)}(e_b)$, where e_b is the quantum bit error rate and $h^{(d)}(x) := -x\log_2(x/(d-1)) - (1-x)\log_2(1-x)$ is the d-dimensional Shannon entropy. Although we do not perform QKD and only measure in the computational basis, the secret key rate formula provides us with a simple and useful parameter that takes both dimensionality and measurement errors into consideration. For a d-dimensional subset of the 55-dimensional space, there are a total of $55!/(55-d)!\,d!$ combinations of possible subspaces. In Fig. 5-(**b**), we show the average and the standard deviation of the secret key rates obtained from a set of 1000 randomly selected d-dimensional subspaces from all possible combinations. Moreover, for a given d-dimensional subspace, we search for combination of states that yields the largest secret

Optics EXPRESS

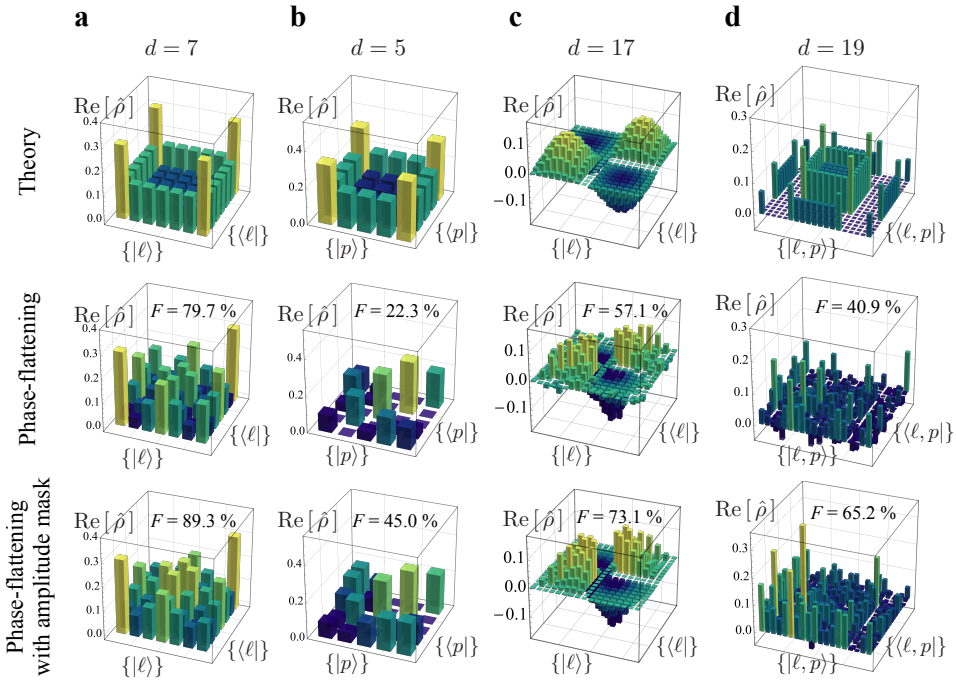

Fig. 7. Simulated tomographically reconstructed density matrices using the phase-flattening-only and the phase-flattening with amplitude masking methods. We show the tomographic reconstruction of (a) the 7-dimensional OAM castle state, (b) the 5-dimensional radial castle state, (c) the 17-dimensional OAM sine state, and (d) the 19-dimensional full-field palace state.

key rates. However, in some cases, the number of possible combinations becomes extremely large, e.g. for a 27-dimensional subset of the 55-dimensional data, there are a total of 3.8×10^{15} possible subsets. Thus, we perform an optimization, consisting of a genetic algorithm, to search among the d-dimensional subsets for the optimal secret key rates, see appendix-c. The maximal secret key rate is found to be 4.19 bits in a 30-dimensional subspace, corresponding to a visibility of 96.8 %, which is well above the error bounds for coherent eavesdropping attacks [8]. The maximum secret key rates found by the genetic algorithm are, on average, 4 standard deviations larger than the mean values from the random sampling. By doing so, we show another aspect of the potential of high-dimensional states for quantum information protocols by allowing for the careful selection of a lower dimensional subset of the complete data.

6. High-dimensional state tomography

As a final test of the versatility and effectiveness of our method, we take on the demanding task of performing high-dimensional quantum state tomography (QST). In particular, we perform our tomographic reconstruction using mutually unbiased bases (MUBs), which are known for dimensions that are power of prime numbers [44]. The measurements of MUBs is an important task in many high-dimensional quantum information protocols, such as QKD [45], channel characterization [46], and high-dimensional entanglement certification [47].

We start by performing QST of a 7-dimensional OAM space. As a non-trivial state to produce in the laboratory, we consider states that are visually interesting, see Fig. 6. In order to avoid

Optics EXPRESS

Table 1. **Comparison of Intensity-Flattening and Phase-Flattening for Measuring Azimuthal and Radial Modes.**

Measurements	d	Intensity-flattening (Experiment)	Phase-flattening (Simulation)	Phase-flattening (AM) (Simulation)
Crosstalk - Radial modes	8	V = 98.3 %	V = 46.6 %	V = 51.0 %
Secret key rate - Full-field	30	R = 4.19 bits	R = 1.34 bits	R = 0.92 bits
QST - Radial modes	5	F = 95.3 %	F = 22.3 %	F = 45.0 %
QST - Azimuthal modes	17	F = 95.4 %	F = 57.1 %	F = 73.1 %
QST - Full-field modes	19	F = 93.8 %	F = 40.9 %	F = 65.2 %

systematic errors in our tomographic reconstruction [48], we experimentally reconstruct the density matrix using a direct inversion given by $\hat{\rho} = \sum_{\alpha,m} P_m^{(\alpha)} \Pi_m^{(\alpha)} - \hat{\mathbb{1}}$, where α labels the MUB, m labels the state, $P_m^{(\alpha)}$ corresponds to the probability of measuring the state $|\psi_m^{(\alpha)}\rangle$ from the MUB α and $\Pi_m^{(\alpha)}$ corresponds to the projector $|\psi_m^{(\alpha)}\rangle\langle\psi_m^{(\alpha)}|$. The experimental generation and reconstruction may be evaluated using the state fidelity given by $F = \left(\mathrm{Tr}\sqrt{\sqrt{\hat{\rho}}\ \hat{\rho}_{\mathrm{th}}\sqrt{\hat{\rho}}}\right)^2$, which reduces to $F = \langle\psi_{\mathrm{th}}|\,\hat{\rho}\,|\psi_{\mathrm{th}}\rangle$ in our case since $\hat{\rho}_{\mathrm{th}}$ are pure states. The experimentally reconstructed 7-dimensional OAM state is shown in Fig. 6-(**a**), along with its theoretical counterpart. The state fidelity is given F = 98.7 %, which shows the high measurement quality of our method for OAM states.

While several techniques have been proposed to measure radial modes, there has been no experimental demonstration of measurements of MUBs for radial modes. To demonstrate the extent of the capability of the intensity-flattening technique, we perform QST of a 5-dimensional state consisting of radial modes ranging from $p = 0$ to $p = 4$ using MUBs. The experimentally reconstructed density matrix, with a corresponding state fidelity of F = 95.3 %, is shown in Fig. 6-(**b**). We note that the highest radial mode, i.e. $p = 4$, corresponds to a mode order of $N_{\mathrm{max}} = 9$. As a comparison, we also perform QST on a 17-dimensional OAM state, where the highest OAM value is $|\ell| = 8$, corresponding to a maximal mode order of $N_{\mathrm{max}} = 9$ as well, see Fig. 6-(**c**). Even in such large dimensions, a relatively high state fidelity of 95.4 % is achieved. Finally, we perform QST on a 19-dimensional state of combined azimuthal and radial modes, see Fig. 6-(**d**). A state fidelity of F = 93.8 % is obtained from the full-field QST showing the full experimental power of our technique.

We now compare the performance of our intensity-flattening method to the previously established phase-flattening method for measuring radial modes of light. In order to compare their performances in terms of azimuthal modes, we simulate the performance of quantum state tomography when using the phase-flattening-only and phase-flattening with amplitude masking techniques. As can be seen from Fig. 7, the state fidelities are significantly lower compared to the case of intensity-flattening, as shown in the main text. As expected, the measurements are particularly bad when measuring radial modes. However, with OAM states that lack certain symmetries, as it is the case here for the *castle*, *sine*, and *palace states*, the phase-flattening technique also performs poorly even when measuring azimuthal modes. Finally, prior to performing QST, we experimentally characterized the coupling efficiency of each measurement setting on SLM-B to compensate for the mode-dependent efficiency associated with intensity-flattening.

Table 1 summarizes how our intensity-flattening technique compares with the well-established phase-flattening methods (with and without amplitude masking), when applied to radial mode

Optics EXPRESS

crosstalk, QKD key rates achievable, and QST of high-dimensional states. Different sets of measurements are compared in terms of visibility (V), secret key rate (R), and state fidelity (F) for several different dimensions (d). The comparison is carried out among intensity-flattening (experimental), phase-flattening (simulated), and phase-flattening with amplitude-masking (simulated). As can be seen, the intensity-flattening method enables significant improvements on all fronts, including a four-fold increase in key rates and vastly better tomographic state fidelities.

7. Conclusion

In conclusion, we have proposed and experimentally demonstrated an intensity-flattening technique which enabled us to projectively measure arbitrary spatial modes with a high level of accuracy. Our method uses a single phase screen, and has the advantage of being simple and straightforward to implement, making it a powerful experimental tool for quantum and classical experiments with the spatial modes of light. In order to demonstrate the versatility of our technique, we have measured radial modes with higher visibilities than ever before – 98.3 % in an 8-dimensional state space. Moreover, we have characterized extremely large high-dimensional states with high visibility by combining the azimuthal and radial modes of LG beams, thus taking advantage of the full information capacity of transverse spatial modes. Finally, as an ultimate test of the generality of this technique, we have performed quantum state tomography on high-dimensional azimuthal and radial modes with significant improvements in fidelity over previous measurement techniques. By enabling the precise measurement of the azimuthal and radial modes of light, our method opens a pathway towards practical quantum and classical communication protocols with record information capacities and levels of security.

Appendix-A

Beam shaping of the backward-propagating beam: In the main text, we have primarily investigated intensity-flattening with a Gaussian backward propagating beam, which is given by the output of the single mode fibre (SMF). However, by manipulating the phase in conjugate planes of the outgoing Gaussian beam, we may shape with high-efficiency the Gaussian beam into a flat-top or an exponential beam at the detection SLM. The flat-top and exponential beams are respectively defined as,

$$E_{\mathrm{ft}}(r,\varphi) = \begin{cases} \frac{1}{w_0}\sqrt{\frac{1}{\pi}} & \text{if } r \le w_0 \\ 0 & \text{if } r > w_0 \end{cases} \tag{3}$$

$$E_{\mathrm{exp}}(r,\varphi) = \frac{1}{w_0}\sqrt{\frac{2}{\pi}}\exp\left(-r/w_0\right). \tag{4}$$

For instance, the flat-top beam has the advantage of being flatter over a certain region of space, compared to the Gaussian beam. However, the fixed extent of the flat-top beam becomes problematic for the higher-order modes that have non-zero intensity at larger radii. On the other hand, the exponential beam is less flat near the origin, but has a larger extent than the Gaussian beam for larger radii. In general, a super-Gaussian beam of the form $\exp\left(-(r/w_0)^n\right)$, may be considered by varying the parameter n by optimizing the trade-off between visibility and efficiency for a given dimension. Indeed, the flat-top, Gaussian and exponential beams are all special cases of super-Gaussian beams with $n = \infty, 2$ and 1, respectively. In Fig. 8, we compare the performance of the previously mentioned beam shapes for measurements of radial modes in dimension 5 and 10. In particular, in dimension 10, for visibilities ranging from $V = 0.98$ to 1, the flat-top beam is more efficient. In the range, $V = 0.83$ to 0.98, the Gaussian beam is more efficient and finally in the range between $V = 0$ and 0.83, exponential beams are more

Optics EXPRESS

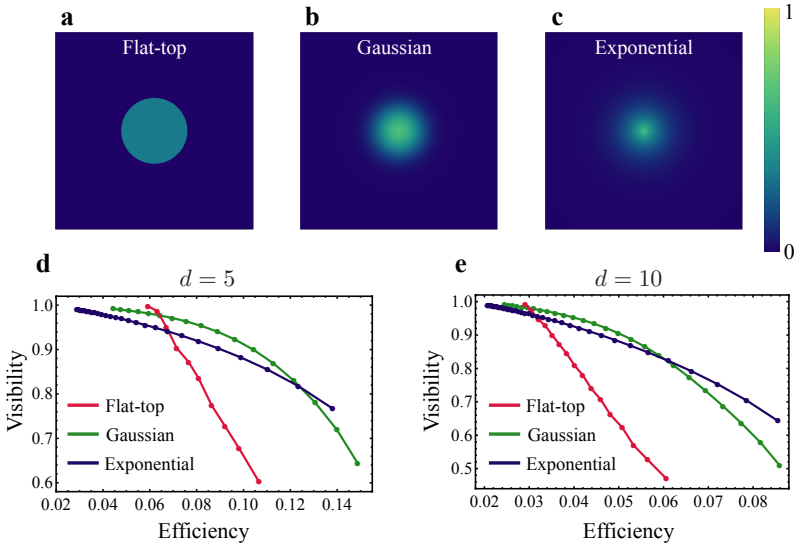

Fig. 8. Comparison of intensity-flattening with different backward-propagating beam. Normalized intensity distribution for three different types of backward propagating beams, i.e. (a) Flat-top, (b) Gaussian and (c) Exponential. The trade-off between visibility and efficiency is shown for all three types of beams in (d) and (e), for dimension 5 and 10, respectively.

efficient. Thus, for a desired range of visibilities and efficiencies, beam shaping of the backward propagating beam consist of an additional mean by which the measurement scheme may be optimized.

Appendix-B

Intensity flattening via induced losses: In the previous section, we have investigated several beam shaping strategies that allows one to achieve higher detection efficiencies for a given range of measurement visibilities. However, in this case, the requirement of beam shaping using phase elements in conjugate planes of the backward propagating beam introduces some complexity to our measurement technique. We now investigate another avenue to achieve a flattening of the backward propagating beam by carefully introducing losses at SLM-B. The losses are introduce in such a way that the Gaussian is cut such that the top region of the Gaussian is made flat. Of course, by doing so, the effect of the Gaussian factor in the overlap integral of LG beams is reduced. In general, this technique is more lossy than simply stretching the Gaussian factor. However, there are cases where a carefully chosen combination of stretching the Gaussian first, then introducing losses in order to cut only the top of the stretched Gaussian may be beneficial in terms of efficiency for a given measurement visibility, see Fig 9.

Appendix-C

Optimal subspaces: As mentioned in the main text, we perform a genetic algorithm in order to obtained the optimal set of state in a given d-dimensional subspace leading to the maximum secret key rates. Considering a population of 10 members, a mutation rate and a mutation frequency of 10 % selected with convergence after a number of iterations ranging from 10,000 and 30,000. The optimal subsets of the full 55-dimensional states are shown in Fig. 10. The list of the azimuthal and radial states considered can be found in Table 2. In Table 2, the label i,

Optics EXPRESS

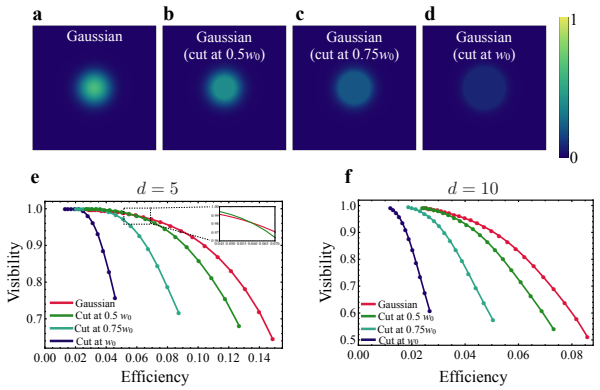

Fig. 9. Comparison of intensity-flattening with different cut of the backward-propagating beam. Normalized intensity distribution for three different types of backward propagating beams with, i.e. (a) no cut (Gaussian), (b) cut at $0.5w_0$, (c) cut at $0.75w_0$ and (d) cut at w_0. The trade-off between visibility and efficiency is shown for all three types of beams in (e) and (f), for dimension 5 and 10, respectively. In dimension 5, we can see in the inset that for visibilities larger than 98.5 %, a cut at $0.5w_0$ increasing the efficiency of the measurement, with respect to an uncut Gaussian.

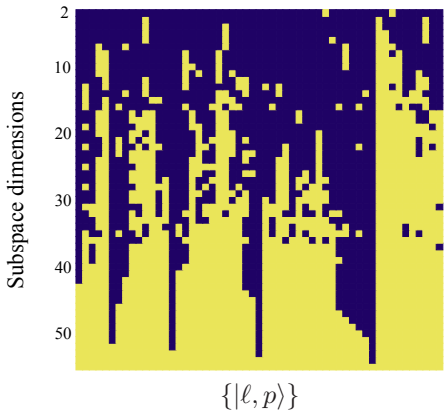

Fig. 10. Optimal d-dimensional subspaces. Representation of the optimal d-dimensional subspaces of the full 55-dimensional measurements. The states on the horizontal axis are explicitly given in Table 2. Yellow indicates the presence of the state in the corresponding subspace, and dark blue indicates its absence.

ranging from 1 to 55, indicates the state employed in order presented in Fig. 5-(a) of the main text. The mode order N, azimuthal index ℓ and radial index p are in the range of 1 to 10, -9 to 9 and 0 to 4, respectively.

Optics EXPRESS

Table 2. **List of the States Considered in the 55-Dimensional Measurements.**

i	N	ℓ	p
1	1	0	0
2	2	-1	0
3	2	1	0
4	3	-2	0
5	3	2	0
6	3	0	1
7	4	-3	0
8	4	3	0
9	4	-1	1
10	4	1	1
11	5	-4	0
12	5	4	0
13	5	-2	1
14	5	2	1
15	5	0	2
16	6	-5	0
17	6	5	0
18	6	-3	1
19	6	3	1
20	6	-1	2
21	6	1	2
22	7	-6	0
23	7	6	0
24	7	-4	1
25	7	4	1
26	7	-2	2
27	7	2	2
28	7	0	3
29	8	-7	0
30	8	7	0
31	8	-5	1
32	8	5	1
33	8	-3	2
34	8	3	2
35	8	-1	3
36	8	1	3
37	9	-8	0
38	9	8	0
39	9	-6	1
40	9	6	1
41	9	-4	2
42	9	4	2
43	9	-2	3
44	9	2	3
45	9	0	4
46	10	-9	0
47	10	9	0
48	10	-7	1
49	10	7	1
50	10	-5	2
51	10	5	2
52	10	-3	3
53	10	3	3
54	10	-1	4
55	10	1	4

Optics EXPRESS

Appendix-D

Castle, Sine, and Palace states: The visually interesting density matrices shown in Fig. 6 of the main text are given by the following states. The 7-dimensional OAM *castle state*, 5-dimensional radial *castle state*, the 17-dimensional OAM *sine state*, and the 19-dimensional full-field *palace states*, are respectively given by the following pure states;

$$|\psi^{(d=7)}_{\text{castle}}\rangle = \frac{1}{\sqrt{\mathcal{N}^{(d=7)}_{\text{castle}}}} \Big(|\ell=-3\rangle + 0.5\,|\ell=-2\rangle + 0.5\,|\ell=-1\rangle + 0.5\,|\ell=0\rangle + 0.5\,|\ell=1\rangle + 0.5\,|\ell=2\rangle + |\ell=3\rangle \Big), \tag{5}$$

$$|\psi^{(d=5)}_{\text{castle}}\rangle = \frac{1}{\sqrt{\mathcal{N}^{(d=5)}_{\text{castle}}}} \Big(|p=0\rangle + 0.6\,|p=1\rangle + 0.6\,|p=2\rangle + 0.6\,|p=3\rangle + |p=4\rangle \Big), \tag{6}$$

$$|\psi^{(d=17)}_{\text{sine}}\rangle = \frac{1}{\sqrt{\mathcal{N}^{(d=17)}_{\text{sine}}}} \sum_{\ell=-8}^{8} \sin\left(2\pi\ell/17\right)|\ell\rangle, \tag{7}$$

$$|\psi^{(d=19)}_{\text{palace}}\rangle = \frac{1}{\sqrt{\mathcal{N}^{(d=19)}_{\text{palace}}}} \Big(0.5|\ell=0,p=0\rangle + 0.8\,|\ell=0,p=1\rangle + 0.5\,|\ell=-3,p=0\rangle + 0.5\,|\ell=3,p=0\rangle + 0.5\,|\ell=-1,p=1\rangle + 0.5\,|\ell=1,p=1\rangle + 0.5\,|\ell=-4,p=0\rangle + 0.5\,|\ell=4,p=0\rangle + 0.5\,|\ell=-2,p=1\rangle + 0.8\,|\ell=2,p=1\rangle + 0.5\,|\ell=3,p=1\rangle \Big), \tag{8}$$

where $\mathcal{N}$ are normalization coefficients.

Funding

Vanier Canada Graduate Scholarships Program; Natural Sciences and Engineering Research Council of Canada (NSERC); Austrian Science Fund (FWF) through the START project Y879-N27; Joint Czech-Austrian project MultiQUEST (I 3053-N27 and GF17-33780L); QuantERA ERA-NET Co-fund (FWF project I 3553-N36); Engineering and Physical Sciences Research Council (EPSRC) (EP/P024114/1).

Acknowledgments

We thank A. Zeilinger and E. Karimi for many fruitful discussions.

Author contributions

F.B. and N.H.V. contributed equally to this work.

Optics EXPRESS

References

1. A. Zeilinger, G. Weihs, T. Jennewein, and M. Aspelmeyer, "Happy centenary, photon," Nature **433**, 230–238 (2005).
2. M. Giustina, M. A. M. Versteegh, S. Wengerowsky, J. Handsteiner, A. Hochrainer, K. Phelan, F. Steinlechner, J. Kofler, J. Larsson, C. Abellán, W. Amaya, V. Pruneri, M. W. Mitchell, J. Beyer, T. Gerrits, A. E. Lita, L. K. Shalm, S. W. Nam, T. Scheidl, R. Ursin, B. Wittmann, and A. Zeilinger, "Significant-loophole-free test of bell's theorem with entangled photons," Phys. Rev. Lett. **115**, 250401 (2015).
3. L. K. Shalm, E. Meyer-Scott, B. G. Christensen, P. Bierhorst, M. A. Wayne, M. J. Stevens, T. Gerrits, S. Glancy, D. R. Hamel, M. S. Allman, K. J. Coakley, S. D. Dyer, C. Hodge, A. E. Lita, V. B. Verma, C. Lambrocco, E. Tortorici, A. L. Migdall, Y. Zhang, D. R. Kumor, W. H. Farr, F. Marsili, M. D. Shaw, J. A. Stern, C. Abellán, W. Amaya, V. Pruneri, T. Jennewein, M. W. Mitchell, P. G. Kwiat, J. C. Bienfang, R. P. Mirin, E. Knill, and S. W. Nam, "Strong loophole-free test of local realism," Phys. Rev. Lett. **115**, 250402 (2015).
4. J. Yin, Y. Cao, Y.-H. Li, J.-G. Ren, S.-K. Liao, L. Zhang, W.-Q. Cai, W.-Y. Liu, B. Li, H. Dai, M. Li, Y.-M. Huang, L. Deng, L. Li, Q. Zhang, N.-L. Liu, Y.-A. Chen, C.-Y. Lu, R. Shu, C.-Z. Peng, J.-Y. Wang, and J.-W. Pan, "Satellite-to-ground entanglement-based quantum key distribution," Phys. Rev. Lett. **119**, 200501 (2017).
5. J. D. Franson, "Bell inequality for position and time," Phys. Rev. Lett. **62**, 2205 (1989).
6. A. K. Jha, M. Malik, and R. W. Boyd, "Exploring energy-time entanglement using geometric phase," Phys. Rev. Lett. **101**, 180405 (2008).
7. S. Walborn and C. Monken, "Transverse spatial entanglement in parametric down-conversion," Phys. Rev. A **76**, 062305 (2007).
8. N. J. Cerf, M. Bourennane, A. Karlsson, and N. Gisin, "Security of quantum key distribution using d-level systems," Phys. Rev. Lett. **88**, 127902 (2002).
9. M. Erhard, R. Fickler, M. Krenn, and A. Zeilinger, "Twisted photons: New quantum perspectives in high dimensions," Light Sci. Appl. **7**, 17146 (2018).
10. M. Krenn, M. Malik, M. Erhard, and A. Zeilinger, "Orbital angular momentum of photons and the entanglement of laguerre–gaussian modes," Phil. Trans. R. Soc. A **375**, 20150442 (2017).
11. L. Allen, L., M. W. Beijersbergen, R. Spreeuw, and J. Woerdman, "Orbital angular momentum of light and the transformation of laguerre-gaussian laser modes," Phys. Rev. A **45**, 8185 (1992).
12. M. Krenn, M. Huber, R. Fickler, R. Lapkiewicz, S. Ramelow, and A. Zeilinger "Generation and confirmation of a (100× 100)-dimensional entangled quantum system," Proc. Natl. Acad. Sci. U.S.A. **111**(17), 6243–6247 (2014).
13. M. Malik, M. Erhard, M. Huber, M. Krenn, R. Fickler, and A. Zeilinger, "Multi-photon entanglement in high dimensions," Nat. Photonics **10**, 248 (2016).
14. F. Cardano, F. Massa, H. Qassim, E. Karimi, S. Slussarenko, D. Paparo, C. de Lisio, F. Sciarrino, E. Santamato, R. W. Boyd, and L. Marrucci, "Quantum walks and wavepacket dynamics on a lattice with twisted photons," Sci. Adv. **1**, e1500087 (2015).
15. G. Vallone, V. D'Ambrosio, A. Sponselli, S. Slussarenko, L. Marrucci, F. Sciarrino, and P. Villoresi, "Free-space quantum key distribution by rotation-invariant twisted photons," Phys. Rev. Lett. **113**, 060503 (2014).
16. M. Mirhosseini, O. S. Magaña-Loaiza, M. N. O'Sullivan, B. Rodenburg, M. Malik, M. P. J. Lavery, M. J. Padgett, D. J. Gauthier, and R. W. Boyd, "High-dimensional quantum cryptography with twisted light," New J. Phys. **17**, 033033 (2015).
17. A. Sit, F. Bouchard, R. Fickler, J. Gagnon-Bischoff, H. Larocque, K. Heshami, D. Elser, C. Peuntinger, K. Günthner, B. Heim, C. Marquardt, G. Leuchs, R. W. Boyd, and E. Karimi, "High-dimensional intracity quantum cryptography with structured photons," Optica **4**(9), 1006–1010 (2017).
18. M. Beijersbergen, R. Coerwinkel, M. Kristensen, and J. Woerdman, "Helical-wavefront laser beams produced with a spiral phaseplate," Opt. Commun. **112**(5), 321–327 (1994).
19. V. Y. Bazhenov, M. Soskin, and M. Vasnetsov, "Screw dislocations in light wavefronts," J. Mod. Opt. **39**(5), 985–990 (1992).
20. N. Heckenberg, R. McDuff, C. Smith, and A. White, "Generation of optical phase singularities by computer-generated holograms," Opt. Lett. **17**(3), 221–223 (1992).
21. L. Marrucci, C. Manzo, and D. Paparo, "Optical spin-to-orbital angular momentum conversion in inhomogeneous anisotropic media," Phys. Rev. Lett. **96**, 163905 (2006).
22. J. P. Kirk and A. L. Jones, "Phase-only complex-valued spatial filter," J. Opt. Soc. Am. **61**(8), 1023–1028 (1971).
23. E. Bolduc, N. Bent, E. Santamato, E. Karimi, and R. W. Boyd, "Exact solution to simultaneous intensity and phase encryption with a single phase-only hologram," Opt. Lett. **38**(18), 3546–3549 (2013).
24. A. Mair, A. Vaziri, G. Weihs, and A. Zeilinger, "Entanglement of the orbital angular momentum states of photons", Nature **412**, 313–316 (2001).
25. H. Qassim,F. M. Miatto, J. P. Torres, M. J. Padgett, E. Karimi, and R. W. Boyd, "Limitations to the determination of a laguerre–gauss spectrum via projective, phase-flattening measurement," J. Opt. Soc. Am. B **31**(6), A20–A23 (2014).
26. G. C. Berkhout, M. P. Lavery, J. Courtial, M. W. Beijersbergen, and M. J. Padgett, "Efficient sorting of orbital angular momentum states of light," Phys. Rev. Lett. **105**, 153601 (2010).
27. M. Mirhosseini, M. Malik, Z. Shi, and R. W. Boyd, "Efficient separation of the orbital angular momentum eigenstates of light," Nat. Commun. **4**, 2781 (2013).
28. N. K. Fontaine, R. Ryf, H. Chen, D. T. Neilson, K. Kim, and J. Carpenter, "Optical spatial mode sorter of azimuthal and radial components," arXiv:1803.04126 (2018).

Optics EXPRESS

29. J. F. Morizur, L. Nicholls, P. Jian, S. Armstrong, N. Treps, N. Hage, M. Hsu, W. Bowen, J. Janousek, and H.-A. Bachor, "Programmable unitary spatial mode manipulation," J. Opt. Soc. Am. A **27**(11), 2524–2531 (2010).
30. F. S. Roux and Y. Zhang, "Projective measurements in quantum and classical optical systems," Phys. Rev. A **90**, 033835 (2014).
31. Y. Zhang, F. S. Roux, M. McLaren, and A. Forbes, "Radial modal dependence of the azimuthal spectrum after parametric down-conversion," Phys. Rev. A **89**, 043820 (2014).
32. E. Karimi and E. Santamato, "Radial coherent and intelligent states of paraxial wave equation," Opt. Lett. **37**(13), 2484–2486 (2012).
33. E. Karimi, R. W. Boyd, P. De La Hoz, H. De Guise, J. Řeháček,Z. Hradil, A. Aiello, G. Leuchs, and L. L. Sánchez-Soto, "Radial quantum number of laguerre-gauss modes," Phys. Rev. A **89**, 063813 (2014).
34. E. Karimi, D. Giovannini, E. Bolduc, N. Bent, F. M. Miatto, M. J. Padgett, and R. W. Boyd, "Exploring the quantum nature of the radial degree of freedom of a photon via hong-ou-mandel interference," Phys. Rev. A **89**, 013829 (2014).
35. W. N. Plick and M. Krenn "Physical meaning of the radial index of laguerre-gauss beams," Phys. Rev. A **92**, 063841 (2015).
36. R. Fickler, M. Ginoya, and R. W. Boyd, "Custom-tailored spatial mode sorting by controlled random scattering," Phys. Rev. B **95**, 161108 (2017).
37. Y. Zhou, M. Mirhosseini, D. Fu, J. Zhao,S. Rafsanjani, H. Mohammad, A. E. Willner, and R. W. Boyd, "Sorting photons by radial quantum number," Phys. Rev. Lett. **119**, 263602 (2017).
38. X. Gu, M. Krenn, M. Erhard, and A. Zeilinger, "Gouy phase radial mode sorter for light: Concepts and experiments," Phys. Rev. Lett. **120**, 103601 (2018).
39. N. Zhao, X. Li, G. Li, and J. M. Kahn, "Capacity limits of spatially multiplexed free-space communication," Nat. Photonics **9**, 822 (2015).
40. J. M. Kahn, G. Li, X. Li, and N. Zhao, "To twist or not to twist: Capacity limits for free-space channels," In Advanced Photonics 2016 (IPR, NOMA, Sensors, Networks, SPPCom, SOF), SpM4E.1 (Optical Society of America, 2016).
41. V. Salakhutdinov, E. Eliel, and W. Löffler, "Full-field quantum correlations of spatially entangled photons," Phys. Rev. Lett. **108**, 173604 (2012).
42. A. Trichili, C. Rosales-Guzmán, A. Dudley, B. Ndagano, A. B. Salem, M. Zghal, and A. Forbes, "Optical communication beyond orbital angular momentum," Sci. Rep. **6**, 27674 (2016).
43. F. Bouchard, A. Sit, K. Heshami, R. Fickler, and E. Karimi, "Round-robin differential-phase-shift quantum key distribution with twisted photons," Phys. Rev. A **98**, 010301 (2018).
44. T. Durt, B.-G. Englert, I. Bengtsson, and K. Życzkowski, "On mutually unbiased bases," Int. J. Quantum Inf. **8**(04), 535–640 (2010).
45. M. Mafu, A. Dudley, S. Goyal, D. Giovannini, M. McLaren, M. J. Padgett, T. Konrad, F. Petruccione, N. Lütkenhaus, and A. Forbes, "Higher-dimensional orbital-angular-momentum-based quantum key distribution with mutually unbiased bases," Phys. Rev. A **88**, 032305 (2013).
46. F. Bouchard, F. Hufnagel, D. Koutnỳ, A. Abbas, A. Sit, K. Heshami, R. Fickler, and E. Karimi, "Full characterization of a high-dimensional quantum communication channel," arXiv:1806.08018 (2018).
47. J. Bavaresco, N. H. Valencia, C. Klöckl, M. Pivoluska, P. Erker, N. Friis, M. Malik, and M. Huber, "Measurements in two bases are sufficient for certifying high-dimensional entanglement," Nat. Phys. **14**, 1032–1037 (2018).
48. C. Schwemmer, L. Knips, D. Richart, H. Weinfurter, T. Moroder, M. Kleinmann, and O. Gühne, "Systematic errors in current quantum state tomography tools," Phys. Rev. Lett. **114**, 080403 (2015).